

1 **The Mechanism of MICU-Dependent Gating of the**
2 **Mitochondrial Ca²⁺ Uniporter**

3 **Authors:** Vivek Garg^{1,*}, Ishan Paranjpe¹, Tiffany Unsulangi¹, Junji Suzuki¹, Lorin S. Milesco²,
4 and Yuriy Kirichok^{1,*}.

5

6 **Affiliations:**

7 ¹Department of Physiology, University of California San Francisco, San Francisco, CA, USA.

8 ²Department of Biology, University of Maryland, College Park, MD, USA.

9 *Correspondence to: yuriy.kirichok@ucsf.edu (YK); vivek.garg@ucsf.edu (VG)

10

11

12 *This Paper is submitted back-to-back with the following paper:*

13 W. Zhuo et al., **Structure of intact human MCU supercomplex with the auxiliary MICU**
14 **subunits**. bioRxiv, 2020.2004.2004.025205 (2020). doi: <https://doi.org/10.1101/2020.04.04.025205>

15

16 **Abstract**

17 Mitochondrial Ca^{2+} uniporter (MCU) mediates mitochondrial Ca^{2+} uptake, regulating ATP
18 production and cell death. According to the existing paradigm, MCU is occluded at the resting
19 cytosolic $[\text{Ca}^{2+}]$ and only opens above an ~ 400 nM threshold. This Ca^{2+} -dependent gating is
20 putatively conferred by MICUs, EF hand-containing auxiliary subunits that block/unblock the
21 MCU pore depending on cytosolic $[\text{Ca}^{2+}]$. Here we provide the first direct, patch-clamp based
22 analysis of the Ca^{2+} -dependent MCU gating and the role played by MICUs. Surprisingly, MICUs
23 do not occlude the MCU pore, and MCU is a constitutively active channel without cytosolic
24 $[\text{Ca}^{2+}]$ activation threshold. Instead, MICUs potentiate MCU activity when cytosolic Ca^{2+} binds
25 to their EF hands. MICUs cause this potentiation by increasing the probability of open state of
26 the MCU channel.

27

28

29 **One Sentence Summary**

30 Auxiliary MICU subunits do not occlude the mitochondrial Ca^{2+} uniporter (MCU) but increase
31 its activity as cytosolic Ca^{2+} is elevated.

32 Main Text

33 Mitochondrial Ca^{2+} uptake regulates ATP production, shapes intracellular Ca^{2+} transients
34 and plays a crucial role in deciding cell fate (*1-4*). It is mediated by the mitochondrial Ca^{2+}
35 uniporter (MCU) (*3-5*), which upon elevation of cytosolic $[\text{Ca}^{2+}]$ ($[\text{Ca}^{2+}]_{\text{cyto}}$) allows selective
36 Ca^{2+} permeation into the mitochondrial matrix, down the high electrochemical gradient across
37 the IMM. All Ca^{2+} channels lose their selectivity and become permeable for Na^+ at low $[\text{Ca}^{2+}]$,
38 when Ca^{2+} is removed from the pore (*6-8*). MCU also conducts Na^+ but only when $[\text{Ca}^{2+}]$ is
39 decreased to low nM range, because the MCU pore has a Ca^{2+} binding site with an exceptionally
40 high affinity ($K_d \leq 2$ nM) (*9-15*). This prevents permeation of abundant cytosolic monovalent
41 cations even at a resting $[\text{Ca}^{2+}]_{\text{cyto}}$ of ~ 100 nM, and makes MCU the most selective Ca^{2+} channel
42 known.

43 MCU activity must be regulated. Insufficient Ca^{2+} uptake would result in deficient ATP
44 production, whereas excessive uptake would lead to mitochondrial Ca^{2+} overload, $\Delta\Psi$
45 dissipation, mitochondrial dysfunction and cell death (*16*). A few early studies suggested that
46 MCU activity might be potentiated by cytosolic $[\text{Ca}^{2+}]$ (*4, 17, 18*). However, the results differed
47 significantly between labs, because MCU activity was assessed indirectly in suspensions of
48 isolated mitochondria and critical experimental conditions could not be reliably controlled (*3, 4*).
49 Thus, such potentiation was controversial and no clear unifying model for Ca^{2+} -dependent MCU
50 gating was generated.

51 Recent molecular characterization established that MCU is a macromolecular complex
52 (fig. S1A). Its pore is formed by the MCU subunit (*19, 20*) and the essential MCU regulator
53 (EMRE) subunit (*21*). EF hand domain-containing auxiliary MICU1–3 subunits are tethered on
54 the cytosolic side of the MCU/EMRE pore (*22, 23*). MICU1 interacts directly with the MCU and

55 EMRE, while MICU2 and MICU3 attach to the MCU complex only by heterodimerizing with
56 MICU1 (21, 24-26). MICU3 is a neuronal- and embryonic-specific isoform with little expression
57 in other tissues (23, 27).

58 The understanding of the molecular composition of the MCU complex renewed interest
59 in the MCU gating by cytosolic Ca^{2+} . In MICU1 deficiency, when none of the MICU subunits is
60 associated with the MCU/EMRE pore, mitochondrial Ca^{2+} ($[\text{Ca}^{2+}]_{\text{mito}}$) starts to increase at lower
61 $[\text{Ca}^{2+}]_{\text{cyto}}$ both in cells (24, 25, 28-31) and isolated mitochondria (32). Based on these results, the
62 term “[Ca^{2+}]_{cyto} threshold for mitochondrial Ca^{2+} uptake” was coined, and it was postulated that
63 MICU1 (in association with other MICUs) confers the $[\text{Ca}^{2+}]_{\text{cyto}}$ threshold for MCU activation
64 (28, 29). Specifically, the current paradigm suggests that at resting $[\text{Ca}^{2+}]_{\text{cyto}}$, MICU1 occludes
65 the MCU pore (28, 33, 34), but when $[\text{Ca}^{2+}]_{\text{cyto}}$ increases above ~400–800 nM and Ca^{2+} binds to
66 the MICU1 EF hands, this occlusion is relieved (24, 28, 29) (Fig. 6A). MICU2 is proposed to
67 facilitate this MICU1 function (24, 25, 35). In this model, the occlusion of MCU by
68 MICU1/MICU2 at the resting $[\text{Ca}^{2+}]_{\text{cyto}}$ is considered well-established (tables S1 and S2), while
69 the degree to which the occlusion is removed at elevated $[\text{Ca}^{2+}]_{\text{cyto}}$ remains controversial with
70 different groups reporting a wide range of effects (tables S1 and S2). *MICU1*^{-/-} mice show
71 profound late embryonic and postnatal lethality (32, 36), while loss-of function MICU1
72 mutations in humans cause fatigue, lethargy, severe myopathy, developmental and learning
73 disabilities, and progressive extrapyramidal movement disorder (30, 37-39).

74 The paradigm that MICUs occlude the MCU pore at resting cytosolic Ca^{2+} and impart
75 $[\text{Ca}^{2+}]_{\text{cyto}}$ activation threshold on MCU has affected the field profoundly. However, it has never
76 been demonstrated by direct measurement of Ca^{2+} currents mediated by MCU. Instead, MCU
77 activity was inferred from the changes in $[\text{Ca}^{2+}]$ inside or outside of mitochondria, as measured

78 with Ca^{2+} indicators. However, such $[\text{Ca}^{2+}]$ changes never reflect MCU activity alone but are
79 determined by the balance between mitochondrial Ca^{2+} uptake and efflux mechanisms (3, 4, 40).
80 Some of these studies (34, 36) used CGP37157 to inhibit the mitochondrial Ca^{2+} efflux
81 associated with the $\text{Ca}^{2+}/\text{Na}^+$ exchange mechanism, but this was clearly insufficient to eliminate
82 all mitochondrial Ca^{2+} efflux. Indeed, if the Ca^{2+} efflux was fully eliminated, the free $[\text{Ca}^{2+}]_{\text{mito}}$
83 (based on the Nernst equation and assuming 100 nM $[\text{Ca}^{2+}]_{\text{cyto}}$ and $\Delta\Psi$ at -160 mV) would reach
84 an enormous value of ~25 mM even with residual MCU activity. Other factors such as $\Delta\Psi$, the
85 volume of mitochondrial matrix, matrix Ca^{2+} buffering with phosphates (40) and pH can further
86 confound indirect assessment of MCU activity using Ca^{2+} indicators.

87 The numerous pitfalls associated with indirect assessment of MCU activity make direct
88 measurements of MCU currents (9, 10, 41) necessary for understanding of MCU regulation and
89 the role of MICU subunits. However, such direct measurements have been considered extremely
90 challenging, especially in the context of structure–function studies of the MCU complex, which
91 require assessment of numerous knockout and mutant models. There have been a few attempts to
92 characterize MICU1-dependent regulation of MCU using direct electrophysiology, but the scope
93 of electrophysiological experiments in these few studies was very limited, and MICU1 function
94 was assessed only at high $[\text{Ca}^{2+}]_{\text{cyto}}$ (42-44). These incomplete electrophysiological studies
95 generated very diverse results ranging from inhibition to no effect of MICU1 on the MCU
96 activity, and thus no clarity was achieved (table S1). One electrophysiological study tried to
97 assess the effects of MICU1 and MICU2 at both low and high $[\text{Ca}^{2+}]_{\text{cyto}}$ (table S1) (25).
98 Unfortunately, in this study a recombinant MCU subunit was reconstituted in planar lipid
99 bilayers in the absence of EMRE, the subunit essential for both a functional MCU channel and
100 the association of MICU1/MICU2 with the MCU pore (25). The observed channel conducted

101 Na⁺ even at μM $[\text{Ca}^{2+}]$ and failed to replicate the exceptionally high MCU selectivity for Ca^{2+} .
102 Thus, the channel activity observed in this EMRE-less system was artifactual.

103 Therefore, to facilitate a rigorous and systematic insight into the function of MICU1–3,
104 as well as other subunits of the MCU complex, we developed a heterologous expression system
105 for direct patch-clamp analysis of the MCU complex in the native IMM. Using this system, we
106 demonstrate that MICUs do not occlude the MCU pore. An accompanying paper by Zhuo et al.,
107 (45) reporting the first complete structure of the human MCU complex, also shows that
108 MICU1/MICU2 are tethered to the periphery of the MCU-EMRE pore and do not occlude the
109 pore. We next demonstrate that the actual function of the MICU subunits is to potentiate MCU
110 activity when their EF hands bind cytosolic Ca^{2+} . Thus, MCU has no intrinsic $[\text{Ca}^{2+}]_{\text{cyto}}$
111 activation threshold. It is a constitutively active channel that is potentiated by $[\text{Ca}^{2+}]_{\text{cyto}}$ via the
112 MICU subunits.

113

114 **Results**

115 **System for direct structure–function analysis of MCU**

116 Two factors are crucial to the success of the whole-IMM patch-clamp: the size of
117 individual mitoplasts (vesicles of the whole native IMM) and the IMM stability during the
118 electrophysiological experiments. Therefore, we tested various cell lines for the best possible
119 optimization of these two factors. Eventually, we selected a *Drp1*^{-/-} MEF cell line (46), in which
120 mitochondria form long tubular networks and provide a significantly higher proportion of large
121 isolated mitoplasts that are also remarkably resilient during the whole-IMM electrophysiological
122 experiments. We confirmed that this cell line expresses all principal subunits of the MCU
123 complex (fig. S2A-D). We next generated gene knockouts for all principal subunits of the MCU

124 complex (MCU, EMRE and MICU1–3) using CRISPR-Cas9 in the background of *Drp1*^{-/-} MEFs
125 (fig. S1). All knockout cell lines lacked protein expression of the respective subunit (fig. S2A-C).

126 To explore the cytosolic/mitochondrial Ca²⁺ phenotypes in these MCU complex knockout
127 cell lines, we induced slow elevation of [Ca²⁺]_{cyto} using the SERCA inhibitor thapsigargin (Tg)
128 and observed an associated increase in [Ca²⁺]_{mito} (fig. S2E-J). [Ca²⁺]_{cyto} was measured using
129 Fura-2 while the mitochondrial Ca²⁺ changes were measured using a genetically-encoded Ca²⁺
130 indicator *Cepia* (47) targeted to mitochondria. [Ca²⁺]_{cyto} under resting conditions was maintained
131 ~75 nM in all cell lines (fig. S2K) and peaked in the range of 400–1000 nM upon addition of Tg
132 (fig. S2L). In cells with the *WT* MCU complex, the [Ca²⁺]_{cyto} increase was followed, after a short
133 delay, by [Ca²⁺]_{mito} elevation (fig. S2E). However, as expected, in *MCU*^{-/-} or *EMRE*^{-/-} cell lines
134 that have no functional MCU complex (19-21), no significant [Ca²⁺]_{mito} elevation was observed
135 (fig. S2F and G). In MICU1–3-deficient cells, the [Ca²⁺]_{cyto} threshold for elevation of [Ca²⁺]_{mito}
136 was altered as compared to that in cells with the *WT* MCU complex (fig. S2H-J, and M). In
137 *MICU1*^{-/-} cells, the threshold was drastically decreased (fig. S2H and M), and a significant but
138 less profound decrease was also observed in *MICU2*^{-/-} cells (fig. S2I and M). However, *MICU3*^{-/-}
139 cells had an increased threshold (fig. S2J and M). Thus, in our cell system, we observed the same
140 [Ca²⁺]_{mito} phenotypes associated with knockout of individual MCU complex subunits as reported
141 previously (24, 25, 28, 29, 34).

142 We next explored how knockouts for various MCU complex subunits affect MCU
143 currents. Importantly, the MCU complex was intact in isolated whole-IMM vesicles (mitoplasts)
144 used in our patch-clamp experiments, and its composition was the same as in intact mitochondria
145 based on MCU-FLAG co-immunoprecipitation experiments (fig. S4A). Mitoplasts isolated from
146 cells with the *WT* MCU complex had a robust whole-IMM Ca²⁺ current (*I*_{Ca}). The voltage step

147 from 0 to -160 mV, followed by a voltage ramp to +80 mV, elicited an inwardly rectifying I_{Ca}
148 that gradually increased as $[Ca^{2+}]_{cyto}$ (bath solution) was elevated (Fig. 1A, *left panel*, and fig.
149 S3A and B). As expected, in a Ca^{2+} -free bath solution (control), we only observed an outward
150 Na^+ current (I_{Na} , black trace) via MCU, because the pipette solution contained Na^+ (Fig. 1A, *left*
151 *panel*, and fig. S3A and B).

152 Mitoplasts isolated from $MCU^{-/-}$ and $EMRE^{-/-}$ lines had no inward I_{Ca} or outward I_{Na} ,
153 confirming the essential role of these two subunits for the functional MCU complex (21, 48, 49)
154 (Fig. 1A and C). Importantly, even millimolar $[Ca^{2+}]_{cyto}$ induced no I_{Ca} in $MCU^{-/-}$ and $EMRE^{-/-}$,
155 demonstrating that MCU is the only electrogenic mechanism for mitochondrial Ca^{2+} uptake.
156 Heterologous expression of MCU or EMRE in their corresponding knockout cell lines (fig. S4B
157 and C) resulted in restoration of the inward I_{Ca} and outward I_{Na} (Fig. 1B and C).

158 Thus, we have identified a system that has robust MCU currents, can be used for
159 heterologous expression of recombinant MCU complex subunits, and significantly improves
160 throughput of whole-IMM patch-clamp recording.

161

162 **MICUs are Ca^{2+} -dependent MCU potentiators**

163 In contrast to $MCU^{-/-}$ and $EMRE^{-/-}$, none of the MICU knockouts (MICU1–3) showed
164 loss of I_{Ca} or I_{Na} (Fig. 1D), demonstrating that these subunits are not absolutely required for a
165 functional MCU channel. However, among all MICU knockouts, loss of MICU1 resulted in a
166 marked reduction (~50%) of I_{Ca} in both micromolar and millimolar ranges of $[Ca^{2+}]_{cyto}$ (Fig. 1D
167 and E, and fig. S5). The same reduction was observed when I_{Ca} was measured at both -160 mV
168 (Fig. 1E) and -80 mV (fig. S5C). We next focused on understanding the mechanism by which
169 MICU1 regulates MCU function.

170 As was suggested previously, MICU1 tethers other MICU subunits to the MCU/EMRE
171 pore (21, 24-26). The accompanying paper reporting the structure of the complete human MCU
172 complex confirms that the MICU1/MICU2 dimer is tethered to the MCU/EMRE pore
173 specifically via interactions between MICU1 and EMRE (Zhuo et al., accompanying manuscript
174 (45)). Thus, in *MICU1*^{-/-} none of the MICU subunits are associated with the MCU complex. The
175 levels of MCU and MCUB (MCU paralog with no Ca²⁺ transport activity and putative dominant-
176 negative effect on the MCU function) subunits (50) were not affected in *MICU1*^{-/-}, while EMRE
177 expression was significantly reduced (fig. S6A-D), as was also shown previously (32). The lower
178 EMRE expression in *MICU1*^{-/-} was not a limiting factor for *I*_{Ca}, because EMRE overexpression
179 in *MICU1*^{-/-} cells did not rescue the *I*_{Ca} reduction (fig. S6D-F). Therefore, the *I*_{Ca} reduction in
180 *MICU1*^{-/-} was caused by the lack of MICU1 (and other MICU proteins) in the MCU complex.
181 Because *I*_{Ca} was recorded at [Ca²⁺]_{cyto} ≥ 10 μM, when the EF hands of MICU subunits (*K*_d ~600
182 nM) (51) are occupied by Ca²⁺, we conclude that in the Ca²⁺-bound state MICUs potentiate the
183 MCU current.

184 We next studied how MICUs affect the MCU current when Ca²⁺ is not bound to their EF
185 hands. Because this requires [Ca²⁺]_{cyto} <60 nM (10-fold less than *K*_d) and *I*_{Ca} cannot be measured
186 reliably under these conditions, we used Na⁺ as the permeating ion. A robust *I*_{Na} via MCU was
187 observed when Ca²⁺ was eliminated on the cytosolic face of the IMM with Ca²⁺ chelators (Fig.
188 2A, *left panel*). As expected, *I*_{Na} completely disappeared in *MCU*^{-/-} and *EMRE*^{-/-} (Fig. 2A and B).
189 Interestingly, in a striking contrast to *I*_{Ca}, *I*_{Na} was not reduced in *MICU1*^{-/-}, (Fig. 2C-E, also see
190 Fig. 1D and E). The very presence of a robust *I*_{Na}, and the fact that it is not altered in *MICU1*^{-/-},
191 argues strongly against the currently accepted paradigm (33, 34) in which the MCU/EMRE pore
192 is occluded by MICUs when their EF hands are not occupied by Ca²⁺ (Fig. 6A). In the absence of

193 cytosolic Ca^{2+} , a robust I_{Na} via MCU was also previously recorded in mitoplasts isolated from
194 COS-7 cells, mouse heart and skeletal muscle (9, 10). Nanomolar concentrations of MCU
195 inhibitor ruthenium red (RuR) completely block this I_{Na} (9, 10). In the absence of divalent
196 cations, a RuR-sensitive, Na^+ -selective MCU-dependent uniport was also reported in intact
197 isolated mitochondria (52, 53). Thus, the MCU/EMRE pore is not occluded by MICU proteins
198 when Ca^{2+} is not bound to their EF hands. Moreover, the similarity of I_{Na} amplitudes in *WT* and
199 *MICU1*^{-/-} (Fig. 2C-E) suggests that in their Ca^{2+} -free state MICUs do not affect ion permeation
200 through the MCU/EMRE pore at all. The accompanying structural paper describing the human
201 MCU complex also demonstrates that MICU1/MICU2 do not occlude the pore entrance.
202 Moreover, the profile of the MCU pore is the same, with or without MICU1/MICU2 attached
203 (Zhuo et al., accompanying manuscript (45)).

204 The *MICU1*^{-/-} phenotypes of I_{Na} (no change) and I_{Ca} (reduction) suggest that the only
205 function of MICUs is potentiation of the MCU complex activity when their EF hands are
206 occupied by Ca^{2+} . To further examine this phenotype, we studied how the ratio of I_{Ca} to I_{Na} , as
207 measured in the same mitoplast, is affected by *MICU1*^{-/-}. Such $I_{\text{Ca}}/I_{\text{Na}}$ ratio depends only on the
208 functional properties of the MCU complex, and, in contrast to I_{Ca} and I_{Na} amplitudes, is
209 independent of the number of MCU complexes in a mitoplast. Thus, an alteration of the $I_{\text{Ca}}/I_{\text{Na}}$
210 ratio in *MICU1*^{-/-} can be directly attributed to altered functional properties of the MCU complex,
211 and would not depend on any associated changes in MCU/EMRE expression affecting the
212 number of MCU complexes.

213 The $I_{\text{Ca}}/I_{\text{Na}}$ ratio was dramatically reduced in *MICU1*^{-/-} mitoplasts (Fig. 2F), which means
214 that the loss of MICUs is directly responsible for the reduction of I_{Ca} as compared to I_{Na} . The loss
215 of MICUs can cause such reduction in the $I_{\text{Ca}}/I_{\text{Na}}$ ratio by either altering the channel gating or

216 affecting the relative affinities for Ca^{2+} and Na^+ binding in the selectivity filter. The reduction in
217 $I_{\text{Ca}}/I_{\text{Na}}$ ratio in *MICUI*^{-/-} could not be explained by altered relative affinities for Ca^{2+} and Na^+
218 binding in the selectivity filter, because I_{Na} was inhibited to the same extent by 2 nM $[\text{Ca}^{2+}]_{\text{cyto}}$ in
219 both *WT* and *MICUI*^{-/-} mitoplasts (Fig. 2G and H). Thus, a reduced $I_{\text{Ca}}/I_{\text{Na}}$ ratio in *MICUI*^{-/-} is
220 caused by a disrupted MICU-dependent gating mechanism. This gating mechanism potentiates
221 MCU currents in a Ca^{2+} -dependent fashion.

222 The above experiments were all performed in cell lines with disrupted *Drp1*. However,
223 *Drp1* is not a part of the MCU complex, and therefore *Drp1* loss is not expected to affect MCU
224 currents as measured directly with patch-clamp electrophysiology. Indeed, in our experiments
225 *Drp1* knockout did not affect the amplitudes of I_{Ca} or I_{Na} mediated by the MCU complex (fig.
226 S7A and B). However, we still confirmed that the observed *MICUI*^{-/-} current phenotypes were
227 the same, irrespective of the *Drp1* background. Similar to MICU1 knockout in *Drp1*^{-/-} MEFs,
228 MICU1 knockout in *Drp1*^{+/+} MEFs did not affect I_{Na} while markedly reduced I_{Ca} (fig. S7C-E).
229 Additionally, *MICUI*^{-/-} reduced the $I_{\text{Ca}}/I_{\text{Na}}$ ratio, as measured in the same mitoplast, to the similar
230 extent in *Drp1*^{+/+} MEFs (fig. S7F). Thus, as expected, *Drp1* presence or absence does not affect
231 currents mediated by the MCU complex or the *MICUI*^{-/-} phenotypes.

232 To conclude, MICU subunits do not occlude the MCU/EMRE pore or impart a $[\text{Ca}^{2+}]_{\text{cyto}}$
233 activation threshold on the MCU complex. Instead, MCU is a constitutively active channel, and
234 the actual function of MICU subunits is to potentiate MCU currents as $[\text{Ca}^{2+}]_{\text{cyto}}$ is elevated.

235

236 **Role of EF hands of MICUs in I_{Ca} potentiation**

237 To confirm that Ca^{2+} binding to the EF hands of MICUs is responsible for the Ca^{2+} -
238 dependent potentiation of MCU, we recombinantly expressed MICU1–3 or MICU1–3 with

239 mutated EF hands (mut-EF-MICU, to disable Ca^{2+} binding (24)) in their respective knockout cell
240 lines and examined the changes in I_{Ca} (Fig. 3A).

241 In $\text{MICU1}^{-/-}$, expression of MICU1 was able to restore I_{Ca} to the *WT* level, but mut-EF-
242 MICU1 expression failed to do so (Fig. 3B). Expression levels of both the recombinant MICU1
243 and mut-EF-MICU1 were significantly higher as compared to MICU1 expression in the cells
244 with *WT* MCU complex (Fig. 3A). This confirms our hypothesis that Ca^{2+} binding to the EF
245 hands of MICU1 is indispensable for I_{Ca} potentiation.

246 In $\text{MICU2}^{-/-}$, I_{Ca} was not significantly affected (Fig. 3C, and 1D and E), because the loss
247 of MICU2 appeared to be compensated with increased MICU1 expression and replacement of
248 MICU1/MICU2 heterodimer with MICU1/MICU1 homodimer (fig. S8A-C). Therefore,
249 overexpression of recombinant MICU2 in $\text{MICU2}^{-/-}$ and preferential conversion of
250 MICU1/MICU1 homodimers back into MICU1/MICU2 heterodimers also did not alter the I_{Ca}
251 amplitude (Fig. 3C). In contrast, mut-EF-MICU2 overexpression displaced MICU1 from
252 MICU1/MICU1 homodimers in favor of MICU1/mut-EF-MICU2 heterodimer, leading to a
253 dominant-negative effect and a significant decrease in MICU-dependent I_{Ca} potentiation (Fig.
254 3C). These functional data, combined with biochemical evidence for MICU1/MICU2
255 heterodimers (25, 54, 55) (also see the companion manuscript by Zhou *et al.*), suggest that
256 MICU2, along with MICU1, is responsible for allosteric potentiation of MCU upon binding of
257 cytosolic Ca^{2+} to their EF hands.

258 The effect of $\text{MICU1}^{-/-}$ on I_{Ca} was more profound as compared to that of $\text{MICU2}^{-/-}$ (Fig.
259 1D and E), because MICU1 could compensate for MICU2. However, the reverse compensation
260 was impossible, because only MICU1 tethers the MICU1/MICU2 heterodimer to the
261 MCU/EMRE pore (Zhuo *et al.*, accompanying manuscript (45)). The composition of MICU

262 dimers can also be affected by MICU3 that similar to MICU2 was proposed to interact and form
263 heterodimers with MICU1 (27). However, in our experiments, we did not observe robust current
264 phenotypes associated with MICU3. Specifically, I_{Ca} was not affected in $MICU3^{-/-}$ mitoplasts,
265 and overexpression of recombinant MICU3 or mut-EF-MICU3 in $MICU3^{-/-}$ also had no effect on
266 I_{Ca} (Fig. 3D). It has been suggested that MICU3 is a minor protein as compared to MICU1 and 2
267 in the majority of tissues and cell lines assessed (27). Although in our system the amount of
268 MICU3 mRNA appeared to be comparable with that of other MICU subunits (fig. S2D), and the
269 MICU3 protein was expressed (Fig. 3A *right panel*, and fig. S2C), the relative abundance of
270 MICU3 vs other MICUs is not clear. Moreover, in contrast to MICU1, MICU3 is not upregulated
271 in $MICU2^{-/-}$ cells (fig. S8B), and thus, MICU3 expression does not appear to be linked to the
272 level of MICU2. Therefore, although MICU3 could in principle support the Ca^{2+} -dependent
273 potentiation of MCU by forming dimers with MICU1 (27), the exact role of MICU3 and its
274 interaction with other MCU complex subunits remains to be established.

275 Ca^{2+} binding to the EF hands of MICU subunits and a subsequent conformational change
276 that potentiates the MCU complex activity require a finite time and may delay I_{Ca}
277 activation/deactivation in response to changes in $[Ca^{2+}]_{cyto}$. Such delayed I_{Ca} kinetics can
278 profoundly affect $[Ca^{2+}]_{mito}$, because in situ MCU takes up Ca^{2+} from Ca^{2+} microdomains (56)
279 that exist in the cytosol only for a few milliseconds (57). Therefore, we examined I_{Ca} activation
280 and deactivation kinetics in response to rapid changes in $[Ca^{2+}]_{cyto}$ and tested whether they
281 depend on MICUs. I_{Ca} activation upon rapid elevation of $[Ca^{2+}]_{cyto}$ from virtually Ca^{2+} -free to 1
282 mM was immediate, with kinetics comparable to the rate of solution exchange ($\tau \sim 0.4$ ms)
283 achieved by our piezoelectric fast application system (Fig. 3E). Importantly, the kinetics of the
284 I_{Ca} rapid response was not altered in $MICU1^{-/-}$ (Fig. 3E and F). The deactivation kinetics was

285 similarly fast and not dependent on MICU1 (Fig. 3E and F). The result of these experiments
286 correspond to the previous observation that EF hands of calmodulin bind Ca^{2+} with a μs time
287 constant (58). The conclusion from these experiments is that the kinetics of Ca^{2+} binding to the
288 MICU's EF hands, and the resultant conformational change in the MCU complex, are extremely
289 fast, and thus MICU-dependent potentiation of the MCU activity should occur instantaneously
290 upon elevation of the $[\text{Ca}^{2+}]_{\text{cyto}}$. This is perhaps true even within Ca^{2+} microdomains, but it has to
291 be taken into account that in our experiments we used somewhat higher $[\text{Ca}^{2+}]_{\text{cyto}}$ (1 mM) as
292 compared to the maximal $[\text{Ca}^{2+}]_{\text{cyto}}$ achieved in the microdomains (100 μM).

293 A phenomenon of Ca^{2+} -induced mitochondrial Ca^{2+} release (mCICR) by which
294 mitochondria release Ca^{2+} into cytosol in response to elevations of $[\text{Ca}^{2+}]_{\text{cyto}}$ has been observed
295 (4, 59, 60). mCICR required mitochondrial depolarization and was proposed to be mediated by
296 MCU (61, 62) and/or the permeability transition pore (PTP) (59, 60). Therefore, we tested
297 whether MCU can mediate Ca^{2+} -dependent Ca^{2+} efflux at depolarized membrane voltages and
298 whether such efflux is dependent on MICUs. We measured outward I_{Ca} at positive voltages with
299 2 mM $[\text{Ca}^{2+}]_{\text{mito}}$ (the pipette solution), as $[\text{Ca}^{2+}]_{\text{cyto}}$ was gradually elevated from virtual zero to 1
300 mM. Remarkably, such $[\text{Ca}^{2+}]_{\text{cyto}}$ elevation failed to induce any outward I_{Ca} . However, as
301 expected, it caused a robust inward I_{Ca} (Fig. 3G). This experiment also demonstrates, as was also
302 suggested previously (9), that MCU has a strong inward rectification (unidirectional Ca^{2+}
303 permeation into the matrix). This strong inward rectification of MCU under various $[\text{Ca}^{2+}]_{\text{cyto}}$
304 remained unaltered in *MICU1*^{-/-} (Fig. 3G). Thus, MCU has a strong preference for conducting
305 Ca^{2+} into mitochondria and is unlikely to mediate Ca^{2+} release via mCICR.

306 It has also been suggested that MCU is regulated by matrix $[\text{Ca}^{2+}]$ (63). Specifically, I_{Ca}
307 was shown to be profoundly reduced at $[\text{Ca}^{2+}]_{\text{mito}} \sim 400$ nM, as compared to that at both lower

308 (Ca^{2+} -free) and higher (high μM) $[\text{Ca}^{2+}]_{\text{mito}}$ (63). The authors also proposed that the reduction of
309 the MCU current at $[\text{Ca}^{2+}]_{\text{mito}} \sim 400$ nM is MICU1-dependent. However, in contrast to this
310 previous observation, in our experiments I_{Ca} amplitude remained unaltered when $[\text{Ca}^{2+}]_{\text{mito}}$ was
311 set at Ca^{2+} -free, 400 nM, or 400 μM (fig. S9). Thus, the MCU complex is not regulated by
312 matrix Ca^{2+} , and MICUs only impart the regulation of the MCU complex by cytosolic Ca^{2+} . It
313 should also be mentioned that the authors proposed a membrane topology of EMRE (63) that is
314 reverse to that determined in the recent biochemical and structural studies (14, 26) (see also the
315 accompanying manuscript by Zhuo et al. (45)).

316 Taken together, these data indicate that MICU proteins allosterically potentiate MCU-
317 mediated Ca^{2+} influx when cytosolic Ca^{2+} binds to their EF hands.

318

319 **MICUs increase the open probability of MCU**

320 To investigate the mechanism by which Ca^{2+} -bound MICU proteins potentiate I_{Ca} , we
321 examined the activity of single MCU channels in inside-out (matrix-side out) IMM patches.
322 Because the unitary Ca^{2+} current (i_{Ca} , current via a single MCU channel) is very small (<1 pA), it
323 must be recorded at high $[\text{Ca}^{2+}] = 105$ mM to improve resolution (9). At this $[\text{Ca}^{2+}]$, EF hands of
324 MICU subunits are fully saturated with Ca^{2+} .

325 MCU exhibits multiple levels of single channel conductance. These subconductances can
326 be observed at all tested voltages (-40, -80, and -120 mV), but their resolution improves
327 markedly as transmembrane voltage becomes more negative. At -120 mV, in addition to what
328 appears to be a fully open i_{Ca} , subconductances at ~ 0.8 and ~ 0.6 of the amplitude of the fully
329 open i_{Ca} can be easily detected (Fig. 4A and C). Because similar amplitude levels were observed
330 in all the patches, we conclude that these events represent genuine subconductances in the MCU

331 channel.

332 There was no difference in the single channel amplitude between control and *MICU1*^{-/-}
333 mitoplasts (Fig. 4A-C). However, we found that the single-channel open probability (P_o) was
334 significantly decreased ~2–3 fold in *MICU1*^{-/-} versus *WT* mitoplasts, depending on the
335 transmembrane voltage (Fig. 4A, B, D and fig. S10A-C). As a result, the time-averaged current
336 contributed by a single MCU channel differs significantly between control and *MICU1*^{-/-}
337 mitoplasts (Fig. 4E), thus mirroring and explaining the effect of MICU1 knockout on the
338 amplitude of the whole-mitoplast I_{Ca} (Fig. 1E).

339 These results demonstrate that the potentiating effect of MICU proteins on the
340 MCU/EMRE pore is not associated with an increased single-channel conductance. Rather, when
341 their EF hands bind Ca^{2+} , MICUs increase MCU currents by causing an increase in the open
342 probability of the MCU/EMRE pore.

343

344 **MICU1 does not affect the Mn^{2+} vs Ca^{2+} permeability of MCU**

345 While Mn^{2+} is essential for the proper function of several mitochondrial enzymes, its
346 excessive accumulation inhibits oxidative phosphorylation and causes toxicity (64). MCU
347 appears to be the primary pathway for Mn^{2+} entry into mitochondria (4). Recently, it has been
348 suggested that MICU1 is responsible for the relatively low permeability of MCU for Mn^{2+} as
349 compared to Ca^{2+} , and MICU1 deficiency or loss-of-function MICU1 mutations in patients can
350 lead to excessive mitochondrial Mn^{2+} accumulation and cellular toxicity (42, 65). These
351 observations were explained within the paradigm in which MICU1 occludes the MCU/EMRE
352 pore. It was postulated that Mn^{2+} binds to MICU1 EF hands but, in contrast to Ca^{2+} , cannot
353 induce the MICU1 conformation change necessary to unblock the MCU pore. Thus, MICU1

354 prevents Mn^{2+} permeation via MCU and ensures selective Ca^{2+} permeation (42, 65).

355 We recorded the inward Mn^{2+} current (I_{Mn}) in the presence of 5 mM $[Mn^{2+}]_{cyto}$. I_{Mn}
356 disappeared in $MCU^{-/-}$ and $EMRE^{-/-}$, confirming that it was solely mediated by MCU (Fig. 5A-
357 D). As was also shown previously (9), I_{Mn} was indeed significantly smaller (~7-fold) than I_{Ca} at 5
358 mM $[Mn^{2+}]_{cyto}$ and 5 mM $[Ca^{2+}]_{cyto}$, respectively (Fig. 5E). However, we also observed that I_{Mn}
359 and I_{Ca} were reduced to a similar extent in $MICU1^{-/-}$ (Fig. 5F-H). This result was in a striking
360 contrast to the current MICU1-based model for Mn^{2+} vs Ca^{2+} selectivity of MCU (42, 65), under
361 which I_{Mn} would be increased but I_{Ca} not affected under our experimental conditions. Moreover,
362 even the ratio between I_{Mn} and I_{Ca} calculated from the same mitoplast (I_{Mn}/I_{Ca}) was not affected
363 in $MICU1^{-/-}$ (Fig. 5I), although it is expected to be decreased as per the MICU1-based model for
364 Mn^{2+} vs Ca^{2+} selectivity of MCU (42, 65). Finally, Mn^{2+} inhibited I_{Ca} to the same extent in *WT*
365 and $MICU1^{-/-}$ mitoplasts (Fig. 5F and J), indicating that Ca^{2+} and Mn^{2+} are likely to compete in
366 the selectivity filter of the MCU/EMRE pore.

367 Thus, the I_{Ca} and I_{Mn} phenotypes of $MICU1^{-/-}$ are the same, and MICU1 does not
368 determine the preference of MCU for Ca^{2+} over Mn^{2+} . Permeation of both Ca^{2+} and Mn^{2+} is
369 enhanced, rather than inhibited by MICU1. Instead of MICU1, the selectivity of the MCU
370 complex for Ca^{2+} over Mn^{2+} (and for any other ion) should be determined by the selectivity filter
371 located in the pore (11-13, 15), exactly as in other ion channels. Thus, the properties of Mn^{2+}
372 permeation via MCU cannot be explained within the paradigm in which MICUs occlude the
373 MCU/EMRE pore, nor it can be used to validate it.

374

375 Discussion

376 In summary, the direct patch-clamp analysis presented here argues for a significant

377 revision of the current paradigm for the gating of the MCU complex, its control by $[Ca^{2+}]_{cyto}$, and
378 the role played by MICU subunits (Fig. 6).

379 In contrast to the existing model, we demonstrated that at low $[Ca^{2+}]_{cyto}$, when EF hands
380 of MICU subunits are Ca^{2+} -free, the MCU/EMRE pore is not occluded by MICUs and conducts
381 robust Na^+ current regardless of MICU's presence. Thus, the MCU complex is a constitutively
382 active channel. We further demonstrated that the real function of MICU subunits is to potentiate
383 the activity of the MCU complex as cytosolic Ca^{2+} is elevated and binds to MICU's EF hands
384 (Fig. 6B). MICU subunits potentiate MCU activity by increasing the open state probability of the
385 MCU/EMRE pore. MICUs are likely to achieve this effect by interacting with EMRE that is
386 predicted to control the gating of the MCU/EMRE pore (14). The structure of the complete MCU
387 complex presented in the accompanying paper clarifies this mechanism further and suggests that
388 MICU1/MICU2 dimers connect (at the cytosolic side) EMREs of two different MCU/EMRE
389 pores and could control MCU gating by pulling on these EMREs (Zhuo et al., accompanying
390 manuscript (45)).

391 MICU1/MICU2 dimer binds cytosolic Ca^{2+} with $K_d \sim 600$ nM (51). To understand the
392 Ca^{2+} -dependent function of the MICU1/MICU2 dimer, the effects of MICUs on the
393 MCU/EMRE pore must be studied at the two extremes of the EF-hand Ca^{2+} titration range –
394 when all MICUs are essentially Ca^{2+} -free and when they are fully occupied by Ca^{2+} . This can be
395 achieved by measuring the two types of currents via the MCU complex - I_{Na} and I_{Ca} .

396 As we demonstrated previously (9, 10) and also elaborate in this work, the MCU complex
397 can conduct both Na^+ and Ca^{2+} . This is because Ca^{2+} and Na^+ have very similar radii and both
398 can bind to and permeate through the narrowest Ca^{2+} binding site in the MCU selectivity filter,
399 similar to other Ca^{2+} channels (6, 11-13). I_{Na} and I_{Ca} have been instrumental in understanding the

400 MCU channel and its exceptionally high Ca^{2+} selectivity (9, 10). I_{Na} is measurable only when
401 $[\text{Ca}^{2+}]_{\text{cyto}} \leq 2 \text{ nM}$ (Fig. 2G), while I_{Ca} can only be measured at $[\text{Ca}^{2+}]_{\text{cyto}} \geq 10 \text{ }\mu\text{M}$ (Fig. 1D). In
402 between 2 nM and 10 μM , lies a $[\text{Ca}^{2+}]_{\text{cyto}}$ range where MCU currents are extremely small and
403 cannot be measured reliably. Such “no-current” range is not a unique property of MCU, but is a
404 characteristic property of all Ca^{2+} -selective channels and is explained by the anomalous mole-
405 fraction effect, a phenomenon of binding and competition between two different ions (Na^+ and
406 Ca^{2+}) in the selectivity filter (66). However, by measuring I_{Na} and I_{Ca} , the patch-clamp
407 electrophysiology can reliably establish the effect of MICUs on the MCU/EMRE pore at the two
408 extremes of the EF-hand Ca^{2+} titration range – when all EF hands are either in the Ca^{2+} -free state
409 or in the Ca^{2+} -occupied state. It is important to understand that such direct measurement of I_{Na}
410 and I_{Ca} is the only reliable way to assess the function of MICU subunits within the MCU
411 complex.

412 It is tempting to assume that optical methods can assess the MCU complex activity and
413 the MICU function continuously over a wide $[\text{Ca}^{2+}]_{\text{cyto}}$ range, starting from high nM. This
414 perceived “high sensitivity” of optical methods is achieved by integration of the net
415 mitochondrial Ca^{2+} influx (even if it is very slow) over a period of time, resulting in a
416 measurable $[\text{Ca}^{2+}]_{\text{mito}}$ change. However, it must be realized that the optical methods do not
417 measure MCU activity directly or in isolation from other Ca^{2+} transport mechanisms, and do not
418 permit adequate control over the experimental conditions. When $[\text{Ca}^{2+}]_{\text{cyto}}$ is in the high nM
419 range (around the resting levels), the MCU-mediated Ca^{2+} uptake is very slow and exists in an
420 equilibrium with the mitochondrial Ca^{2+} efflux mechanisms (40). Thus, any measured changes in
421 $[\text{Ca}^{2+}]_{\text{mito}}$ cannot be assigned to MCU exclusively. When $[\text{Ca}^{2+}]_{\text{cyto}}$ is elevated into the μM range,
422 the MCU activity becomes high and overwhelms not only the Ca^{2+} efflux machinery but also the

423 electron transport chain, resulting in a decreased driving force for Ca^{2+} and underestimation of
424 the MCU activity (3, 4). Because of all these technical limitations, measuring the effect of MICU
425 knockouts on I_{Na} at nM $[\text{Ca}^{2+}]_{\text{cyto}}$ and on I_{Ca} at μM $[\text{Ca}^{2+}]_{\text{cyto}}$ with direct patch-clamp
426 electrophysiology is the only way to reliably study the MICU function.

427 Here we demonstrate that the MCU complex is constitutively active and has no intrinsic
428 $[\text{Ca}^{2+}]_{\text{cyto}}$ threshold. A recent report also suggested no apparent $[\text{Ca}^{2+}]_{\text{cyto}}$ threshold for MCU in
429 heart and skeletal muscle (67). Thus, the $[\text{Ca}^{2+}]_{\text{cyto}}$ threshold for elevation of $[\text{Ca}^{2+}]_{\text{mito}}$ is simply
430 determined by the equilibrium between the MCU-dependent Ca^{2+} uptake and the mitochondrial
431 Ca^{2+} efflux mechanisms. Such a simple equilibrium-based $[\text{Ca}^{2+}]_{\text{cyto}}$ threshold for $[\text{Ca}^{2+}]_{\text{mito}}$
432 elevation was proposed previously and was termed the “set point” (40).

433 Assuming that the K_d for Ca^{2+} binding to MICU EF hands is ~ 600 nM (51), MICUs
434 would start potentiating the MCU complex activity already in the high nanomolar range of
435 $[\text{Ca}^{2+}]_{\text{cyto}}$, around the resting levels. Thus, MICUs should help MCU to overcome the
436 mitochondrial Ca^{2+} efflux machinery and decrease the set point.

437 It is therefore paradoxical that the optical studies report not an increase but a decrease in
438 “threshold” for mitochondrial Ca^{2+} uptake in *MICU1*^{-/-}. However, it simply illustrates that the
439 results of the optical experiments should be interpreted with a caution not only at the level of
440 MCU but also at the level of the whole organelle. The set point for mitochondrial Ca^{2+}
441 accumulation is affected not only by the MCU-mediated uptake but also by mitochondrial Ca^{2+}
442 efflux and numerous other factors such as $\Delta\psi$, matrix pH, permeability of the outer
443 mitochondrial membrane, and mitochondria-ER interface, to mention the most obvious. These
444 factors can also change and overcompensate for the reduced MCU activity in *MICU1*^{-/-}, resulting
445 in a decreased set point. In contrast to the *MICU1*^{-/-}, such overcompensation, however, cannot

446 correct the phenotype of MCU and EMRE knockouts because the mitochondrial Ca^{2+} uptake is
447 completely eliminated. To further illustrate these points, in species other than mammals, where
448 the compensatory mechanisms induced by MICU1 knockout may be different, the $[\text{Ca}^{2+}]_{\text{cyto}}$
449 “threshold” for $[\text{Ca}^{2+}]_{\text{mito}}$ elevation is affected in a different way, although the composition of the
450 MCU complex (including EMRE and MICU1) is similar to mammals. Specifically, in
451 *Trypanosoma cruzi*, MICU1 knockout causes an increase in the Ca^{2+} uptake “threshold” and a
452 marked decrease in Ca^{2+} uptake capacity at all $[\text{Ca}^{2+}]_{\text{cyto}}$ (68). The possibility that MICU proteins
453 have other functions (69) beyond being a part of the MCU complex can further complicate the
454 interpretation of the *MICU1*^{-/-} phenotype as assessed by optical methods. In *Drosophila*, a lethal
455 phenotype of MICU1 knockout was not rescued when combined with either MCU or EMRE
456 knockouts (the MCU and EMRE knockouts themselves had mild phenotypes), suggesting
457 functions for MICU proteins beyond the MCU complex (69). Thus, the results obtained with
458 optical methods must be interpreted with due consideration to direct electrophysiological and
459 structural data on the MCU complex. Otherwise, not only the properties of the MCU complex,
460 but also mitochondrial Ca^{2+} homeostasis in general will be misunderstood.

461 In summary, we demonstrate that MICUs are Ca^{2+} -dependent MCU potentiators. They
462 are likely to exert their potentiating effect over a range of $[\text{Ca}^{2+}]_{\text{cyto}}$ from resting to high
463 micromolar. By doing so, MICUs can control both the $[\text{Ca}^{2+}]_{\text{cyto}}$ set point for $[\text{Ca}^{2+}]_{\text{mito}}$ elevation
464 and the maximum $[\text{Ca}^{2+}]_{\text{mito}}$ reached during intracellular Ca^{2+} signaling. Importantly, the
465 potentiation of MCU by MICUs could help to reduce the number of MCU channels required for
466 adequate Ca^{2+} -dependent stimulation of mitochondrial ATP production. Without MICUs, the
467 number of MCU channels per mitochondrion would have to be ~2 times higher, which would
468 also increase futile Ca^{2+} cycling at resting $[\text{Ca}^{2+}]_{\text{cyto}}$.

469 **REFERENCES AND NOTES**

- 470 1. B. Glancy, R. S. Balaban, Role of mitochondrial Ca²⁺ in the regulation of cellular energetics.
471 *Biochemistry* **51**, 2959-2973 (2012).
472
- 473 2. M. J. Berridge, M. D. Bootman, H. L. Roderick, Calcium signalling: dynamics, homeostasis and
474 remodelling. *Nature reviews* **4**, 517-529 (2003).
475
- 476 3. P. Bernardi, Mitochondrial transport of cations: channels, exchangers, and permeability
477 transition. *Physiol Rev* **79**, 1127-1155 (1999).
478
- 479 4. T. E. Gunter, D. R. Pfeiffer, Mechanisms by which mitochondria transport calcium. *Am J Physiol*
480 **258**, C755-786 (1990).
481
- 482 5. H. F. Deluca, G. W. Engstrom, Calcium uptake by rat kidney mitochondria. *Proc Natl Acad Sci U S*
483 *A* **47**, 1744-1750 (1961).
484
- 485 6. L. Tang *et al.*, Structural basis for Ca²⁺ selectivity of a voltage-gated calcium channel. *Nature* **505**,
486 56-61 (2014).
487
- 488 7. P. Hess, J. B. Lansman, R. W. Tsien, Calcium channel selectivity for divalent and monovalent
489 cations. Voltage and concentration dependence of single channel current in ventricular heart
490 cells. *J Gen Physiol* **88**, 293-319 (1986).
491
- 492 8. P. Hess, R. W. Tsien, Mechanism of ion permeation through calcium channels. *Nature* **309**, 453-
493 456 (1984).
494
- 495 9. Y. Kirichok, G. Krapivinsky, D. E. Clapham, The mitochondrial calcium uniporter is a highly selective
496 ion channel. *Nature* **427**, 360-364 (2004).
497
- 498 10. F. Fieni, S. B. Lee, Y. N. Jan, Y. Kirichok, Activity of the mitochondrial calcium uniporter varies
499 greatly between tissues. *Nat Commun* **3**, 1317 (2012).
500
- 501 11. N. X. Nguyen *et al.*, Cryo-EM structure of a fungal mitochondrial calcium uniporter. *Nature* **559**,
502 570-574 (2018).
503
- 504 12. C. Fan *et al.*, X-ray and cryo-EM structures of the mitochondrial calcium uniporter. *Nature* **559**,
505 575-579 (2018).
506
- 507 13. R. Baradaran, C. Wang, A. F. Siliciano, S. B. Long, Cryo-EM structures of fungal and metazoan
508 mitochondrial calcium uniporters. *Nature* **559**, 580-584 (2018).
509
- 510 14. Y. Wang *et al.*, Structural Mechanism of EMRE-Dependent Gating of the Human Mitochondrial
511 Calcium Uniporter. *Cell* **177**, 1252-1261 e1213 (2019).
512
- 513 15. J. Yoo *et al.*, Cryo-EM structure of a mitochondrial calcium uniporter. *Science* **361**, 506-511 (2018).
514

- 515 16. P. Bernardi, A. Rasola, Calcium and cell death: the mitochondrial connection. *Subcell Biochem* **45**,
516 481-506 (2007).
517
- 518 17. H. Kroner, Ca²⁺ ions, an allosteric activator of calcium uptake in rat liver mitochondria. *Arch*
519 *Biochem Biophys* **251**, 525-535 (1986).
520
- 521 18. A. Vinogradov, A. Scarpa, The initial velocities of calcium uptake by rat liver mitochondria. *J Biol*
522 *Chem* **248**, 5527-5531 (1973).
523
- 524 19. J. M. Baughman *et al.*, Integrative genomics identifies MCU as an essential component of the
525 mitochondrial calcium uniporter. *Nature* **476**, 341-345 (2011).
526
- 527 20. D. De Stefani, A. Raffaello, E. Teardo, I. Szabo, R. Rizzuto, A forty-kilodalton protein of the inner
528 membrane is the mitochondrial calcium uniporter. *Nature* **476**, 336-340 (2011).
529
- 530 21. Y. Sancak *et al.*, EMRE is an essential component of the mitochondrial calcium uniporter complex.
531 *Science* **342**, 1379-1382 (2013).
532
- 533 22. F. Perocchi *et al.*, MICU1 encodes a mitochondrial EF hand protein required for Ca²⁺ uptake.
534 *Nature* **467**, 291-296 (2010).
535
- 536 23. M. Plovanich *et al.*, MICU2, a paralog of MICU1, resides within the mitochondrial uniporter
537 complex to regulate calcium handling. *PLoS One* **8**, e55785 (2013).
538
- 539 24. K. J. Kamer, V. K. Mootha, MICU1 and MICU2 play nonredundant roles in the regulation of the
540 mitochondrial calcium uniporter. *EMBO Rep* **15**, 299-307 (2014).
541
- 542 25. M. Patron *et al.*, MICU1 and MICU2 finely tune the mitochondrial Ca²⁺ uniporter by exerting
543 opposite effects on MCU activity. *Mol Cell* **53**, 726-737 (2014).
544
- 545 26. M. F. Tsai *et al.*, Dual functions of a small regulatory subunit in the mitochondrial calcium
546 uniporter complex. *eLife* **5**, (2016).
547
- 548 27. M. Patron, V. Granatiero, J. Espino, R. Rizzuto, D. De Stefani, MICU3 is a tissue-specific enhancer
549 of mitochondrial calcium uptake. *Cell Death Differ* **26**, 179-195 (2019).
550
- 551 28. K. Mallilankaraman *et al.*, MICU1 is an essential gatekeeper for MCU-mediated mitochondrial
552 Ca²⁺ uptake that regulates cell survival. *Cell* **151**, 630-644 (2012).
553
- 554 29. G. Csordas *et al.*, MICU1 controls both the threshold and cooperative activation of the
555 mitochondrial Ca²⁺(+) uniporter. *Cell Metab* **17**, 976-987 (2013).
556
- 557 30. C. V. Logan *et al.*, Loss-of-function mutations in MICU1 cause a brain and muscle disorder linked
558 to primary alterations in mitochondrial calcium signaling. *Nat Genet* **46**, 188-193 (2014).
559
- 560 31. S. de la Fuente, J. Matesanz-Isabel, R. I. Fonteriz, M. Montero, J. Alvarez, Dynamics of
561 mitochondrial Ca²⁺ uptake in MICU1-knockdown cells. *Biochem J* **458**, 33-40 (2014).

- 562 32. J. C. Liu *et al.*, MICU1 Serves as a Molecular Gatekeeper to Prevent In Vivo Mitochondrial Calcium
563 Overload. *Cell Rep* **16**, 1561-1573 (2016).
564
- 565 33. C. B. Phillips, C. W. Tsai, M. F. Tsai, The conserved aspartate ring of MCU mediates MICU1 binding
566 and regulation in the mitochondrial calcium uniporter complex. *eLife* **8**, (2019).
567
- 568 34. M. Paillard *et al.*, MICU1 Interacts with the D-Ring of the MCU Pore to Control Its Ca(2+) Flux and
569 Sensitivity to Ru360. *Mol Cell* **72**, 778-785 e773 (2018).
570
- 571 35. J. Matesanz-Isabel *et al.*, Functional roles of MICU1 and MICU2 in mitochondrial Ca(2+) uptake.
572 *Biochim Biophys Acta* **1858**, 1110-1117 (2016).
573
- 574 36. A. N. Antony *et al.*, MICU1 regulation of mitochondrial Ca(2+) uptake dictates survival and tissue
575 regeneration. *Nat Commun* **7**, 10955 (2016).
576
- 577 37. D. Lewis-Smith *et al.*, Homozygous deletion in MICU1 presenting with fatigue and lethargy in
578 childhood. *Neurol Genet* **2**, e59 (2016).
579
- 580 38. S. Musa *et al.*, A Middle Eastern Founder Mutation Expands the Genotypic and Phenotypic
581 Spectrum of Mitochondrial MICU1 Deficiency: A Report of 13 Patients. *JIMD Rep* **43**, 79-83 (2019).
582
- 583 39. G. Bhosale *et al.*, Pathological consequences of MICU1 mutations on mitochondrial calcium
584 signalling and bioenergetics. *Biochim Biophys Acta* **1864**, 1009-1017 (2017).
585
- 586 40. D. G. Nicholls, Mitochondria and calcium signaling. *Cell Calcium* **38**, 311-317 (2005).
587
- 588 41. V. Garg, Y. Y. Kirichok, Patch-Clamp Analysis of the Mitochondrial Calcium Uniporter. *Methods*
589 *Mol Biol* **1925**, 75-86 (2019).
590
- 591 42. K. J. Kamer *et al.*, MICU1 imparts the mitochondrial uniporter with the ability to discriminate
592 between Ca(2+) and Mn(2+). *Proc Natl Acad Sci U S A* **115**, E7960-E7969 (2018).
593
- 594 43. H. Vais *et al.*, EMRE Is a Matrix Ca(2+) Sensor that Governs Gatekeeping of the Mitochondrial
595 Ca(2+) Uniporter. *Cell Rep* **14**, 403-410 (2016).
596
- 597 44. N. E. Hoffman *et al.*, MICU1 motifs define mitochondrial calcium uniporter binding and activity.
598 *Cell Rep* **5**, 1576-1588 (2013).
599
- 600 45. W. Zhuo *et al.*, Structure of intact human MCU supercomplex with the auxiliary MICU subunits.
601 *bioRxiv*, 2020.2004.2004.025205 (2020).
602
- 603 46. N. Ishihara *et al.*, Mitochondrial fission factor Drp1 is essential for embryonic development and
604 synapse formation in mice. *Nat Cell Biol* **11**, 958-966 (2009).
605
- 606 47. J. Suzuki *et al.*, Imaging intraorganellar Ca²⁺ at subcellular resolution using CEPIA. *Nat Commun*
607 **5**, 4153 (2014).
608

- 609 48. X. Pan *et al.*, The physiological role of mitochondrial calcium revealed by mice lacking the
610 mitochondrial calcium uniporter. *Nat Cell Biol* **15**, 1464-1472 (2013).
611
- 612 49. E. Kovacs-Bogdan *et al.*, Reconstitution of the mitochondrial calcium uniporter in yeast. *Proc Natl*
613 *Acad Sci U S A* **111**, 8985-8990 (2014).
614
- 615 50. A. Raffaello *et al.*, The mitochondrial calcium uniporter is a multimer that can include a dominant-
616 negative pore-forming subunit. *Embo J* **32**, 2362-2376 (2013).
617
- 618 51. K. J. Kamer, Z. Grabarek, V. K. Mootha, High-affinity cooperative Ca(2+) binding by MICU1-MICU2
619 serves as an on-off switch for the uniporter. *EMBO Rep* **18**, 1397-1411 (2017).
620
- 621 52. P. Bernardi, A. Angrilli, G. F. Azzone, A gated pathway for electrophoretic Na⁺ fluxes in rat liver
622 mitochondria. Regulation by surface Mg²⁺. *Eur J Biochem* **188**, 91-97 (1990).
623
- 624 53. J. P. Wehrle, M. Jurkowitz, K. M. Scott, G. P. Brierley, Mg²⁺ and the permeability of heart
625 mitochondria to monovalent cations. *Arch Biochem Biophys* **174**, 313-323 (1976).
626
- 627 54. C. Petrunaro *et al.*, The Ca(2+)-Dependent Release of the Mia40-Induced MICU1-MICU2 Dimer
628 from MCU Regulates Mitochondrial Ca(2+) Uptake. *Cell Metab* **22**, 721-733 (2015).
629
- 630 55. Y. Xing *et al.*, Dimerization of MICU Proteins Controls Ca(2+) Influx through the Mitochondrial
631 Ca(2+) Uniporter. *Cell Rep* **26**, 1203-1212 e1204 (2019).
632
- 633 56. R. Rizzuto *et al.*, Close contacts with the endoplasmic reticulum as determinants of mitochondrial
634 Ca²⁺ responses. *Science* **280**, 1763-1766 (1998).
635
- 636 57. E. Neher, Vesicle pools and Ca²⁺ microdomains: new tools for understanding their roles in
637 neurotransmitter release. *Neuron* **20**, 389-399 (1998).
638
- 639 58. G. C. Faas, S. Raghavachari, J. E. Lisman, I. Mody, Calmodulin as a direct detector of Ca²⁺ signals.
640 *Nat Neurosci* **14**, 301-304 (2011).
641
- 642 59. P. Bernardi, V. Petronilli, The permeability transition pore as a mitochondrial calcium release
643 channel: a critical appraisal. *J Bioenerg Biomembr* **28**, 131-138 (1996).
644
- 645 60. F. Ichas, L. S. Jouaville, J. P. Mazat, Mitochondria are excitable organelles capable of generating
646 and conveying electrical and calcium signals. *Cell* **89**, 1145-1153 (1997).
647
- 648 61. M. Montero, M. T. Alonso, A. Albillos, J. Garcia-Sancho, J. Alvarez, Mitochondrial Ca(2+)-induced
649 Ca(2+) release mediated by the Ca(2+) uniporter. *Mol Biol Cell* **12**, 63-71 (2001).
650
- 651 62. U. Igbavboa, D. R. Pfeiffer, Regulation of reverse uniport activity in mitochondria by
652 extramitochondrial divalent cations. Dependence on a soluble intermembrane space component.
653 *J Biol Chem* **266**, 4283-4287 (1991).
654
- 655 63. H. Vais *et al.*, EMRE Is a Matrix Ca(2+) Sensor that Governs Gatekeeping of the Mitochondrial
Ca(2+) Uniporter. *Cell reports* **14**, 403-410 (2016).

- 657 64. T. E. Gunter *et al.*, An analysis of the effects of Mn²⁺ on oxidative phosphorylation in liver, brain,
658 and heart mitochondria using state 3 oxidation rate assays. *Toxicol Appl Pharmacol* **249**, 65-75
659 (2010).
660
- 661 65. J. Wettmarshausen *et al.*, MICU1 Confers Protection from MCU-Dependent Manganese Toxicity.
662 *Cell Rep* **25**, 1425-1435 e1427 (2018).
663
- 664 66. B. Hille, *Ionic channels of excitable membranes*. (Sinauer Associates, Sunderland, Mass., ed. 2nd,
665 1992), pp. xiii, 607.
666
- 667 67. A. P. Wescott, J. P. Y. Kao, W. J. Lederer, L. Boyman, Voltage-energized calcium-sensitive ATP
668 production by mitochondria. *Nature Metabolism* **1**, 975-984 (2019).
669
- 670 68. M. S. Bertolini, M. A. Chiurillo, N. Lander, A. E. Vercesi, R. Docampo, MICU1 and MICU2 Play an
671 Essential Role in Mitochondrial Ca(2+) Uptake, Growth, and Infectivity of the Human Pathogen
672 *Trypanosoma cruzi*. *MBio* **10**, (2019).
673
- 674 69. R. Tufi *et al.*, Comprehensive Genetic Characterization of Mitochondrial Ca(2+) Uniporter
675 Components Reveals Their Different Physiological Requirements In Vivo. *Cell Rep* **27**, 1541-1550
676 e1545 (2019).
677
- 678 70. F. A. Ran *et al.*, Genome engineering using the CRISPR-Cas9 system. *Nat Protoc* **8**, 2281-2308
679 (2013).
680
- 681 71. G. Grynkiewicz, M. Poenie, R. Y. Tsien, A new generation of Ca²⁺ indicators with greatly improved
682 fluorescence properties. *J Biol Chem* **260**, 3440-3450 (1985).
683
- 684 72. D. A. Winter, *Biomechanics and motor control of human movement*. (Wiley, Hoboken, N.J., ed.
685 4th, 2009), pp. xiv, 370 pages.
686
- 687 73. D. D. Hall, Y. Wu, F. E. Domann, D. R. Spitz, M. E. Anderson, Mitochondrial calcium uniporter
688 activity is dispensable for MDA-MB-231 breast carcinoma cell survival. *PLoS One* **9**, e96866 (2014).
689
- 690 74. G. Bhosale *et al.*, Pathological consequences of MICU1 mutations on mitochondrial calcium
691 signalling and bioenergetics. *Biochim Biophys Acta Mol Cell Res* **1864**, 1009-1017 (2017).
692

693 ACKNOWLEDGEMENTS

694 We thank Drs. Katsuyoshi Mihara (Kyushu University, Japan) and David C. Chan (Caltech,
695 USA) for sending us *Drp1*^{-/-} MEFs, and Dr. Toren Finkel (University of Pittsburgh, USA) for
696 sending the MEFs with intact Drp1 (*WT* and *MICUI*^{-/-} MEFs). We thank the Nikon Microscopy
697 Core (DeLaine Larsen, Kari Herrington) and Lab for Cell Analysis (Sarah Elms) at UCSF for
698 help with use of microscopy and FACS equipment. We thank all members of the Y.K. lab for
699 helpful discussions; **Funding:** This work was supported by American Heart Association
700 Scientist Development Grant 17SDG33660926 (V.G.) and NIH grant 5R01GM107710 (Y.K.);
701 **Author contributions:** V.G. and Y.K. conceived the project and designed all experiments. V.G.
702 performed all experiments. V.G. and T.U. performed Western blot experiments. J.S. consulted on
703 Ca²⁺ imaging experiments. I.P. helped with the analysis of Ca²⁺ imaging experiments. L.S.M.
704 consulted on single-channel analysis using QuB. V.G and Y.K. discussed the results and wrote
705 the manuscript. All authors commented on the manuscript; **Competing interests:** Authors
706 declare no competing interests; **Data and materials availability:** All data is available in the
707 main text or the supplementary materials. Further information and requests for reagents may be
708 directed to the lead contact Yuriy Kirichok (yuriy.kirichok@ucsf.edu).

709

710 SUPPLEMENTARY MATERIALS

711 Materials and Methods

712 Figure S1 – S10

713 Tables S1 – S2

714 References

715 **FIGURES**

716 **Fig. 1. MCU-mediated I_{Ca} in *WT* and knockouts of MCU complex subunits.** (A) Inward I_{Ca}
717 elicited by a voltage ramp in *WT*, *MCU*^{-/-} and *EMRE*^{-/-} mitoplasts exposed to $[Ca^{2+}]_{cyto}$ of 30 μ M,
718 100 μ M and 1 mM. In *WT*, also note an outward Na^+ current via MCU at positive voltages in
719 Ca^{2+} -free bath solution (Control). Voltage protocol is indicated on the top. (B) I_{Ca} is rescued by
720 the recombinant expression of MCU and EMRE in their respective knockout cell lines. (C) I_{Ca}
721 density measured at -160 mV at different $[Ca^{2+}]_{cyto}$ in indicated cell lines. ($n = 4$ to 5 each) Mean
722 \pm SEM. (D) Inward I_{Ca} in *WT*, *MICU1*^{-/-}, *MICU2*^{-/-} and *MICU3*^{-/-} mitoplasts exposed to 10 μ M,
723 100 μ M and 1 mM $[Ca^{2+}]_{cyto}$. (E) I_{Ca} amplitudes measured at -160 mV in mitoplasts at $[Ca^{2+}]_{cyto}$
724 of 10 μ M, 100 μ M and 1 mM (*upper*), as well as 5 mM and 25 mM (*lower*). ($n = 8$ to 17) Mean
725 \pm SEM; one-way ANOVA with post-hoc Tuckey test. ** $p < 0.01$; *** $p < 0.001$.

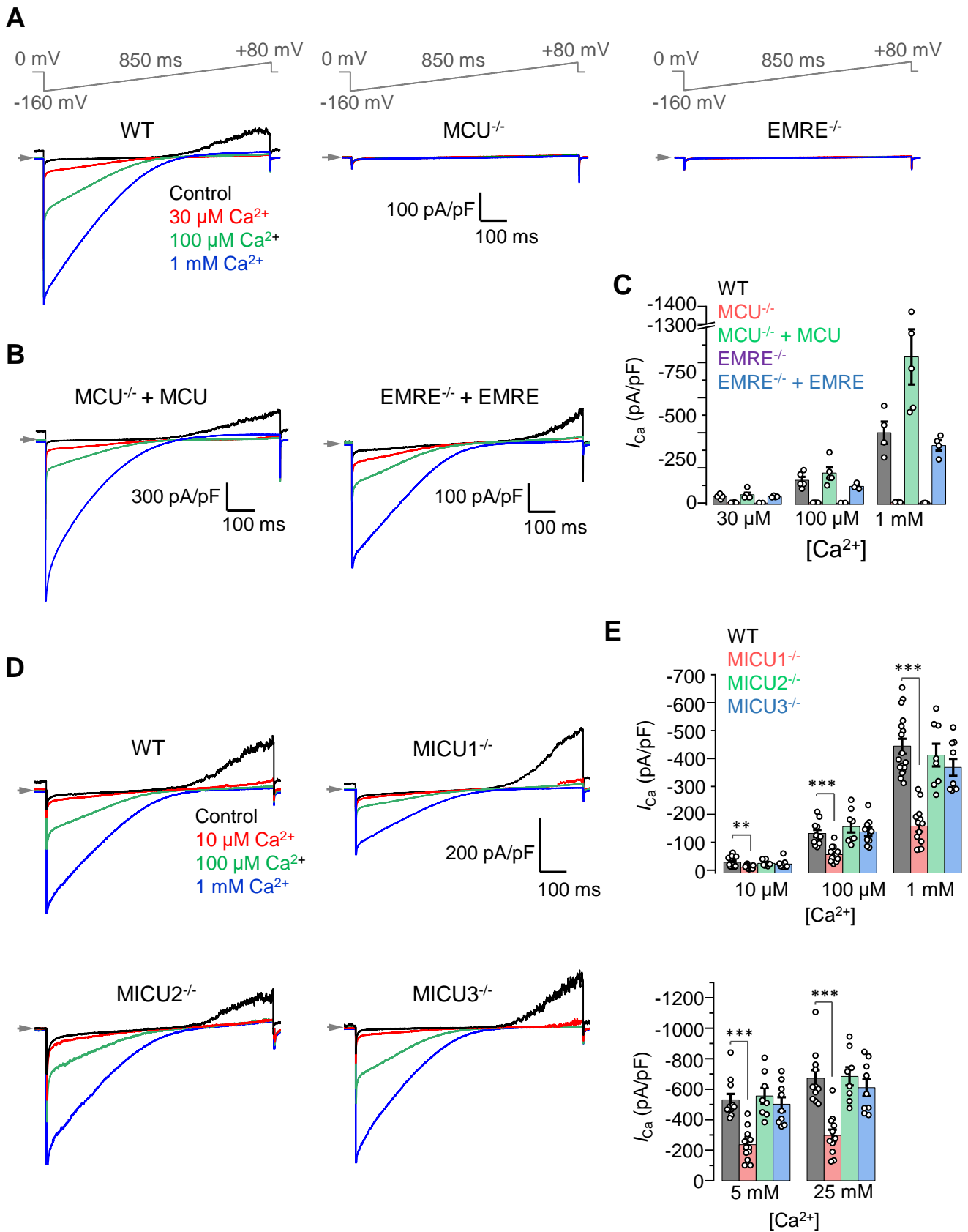


Fig. 1

726 **Fig. 2. MICU1 is a Ca²⁺-dependent MCU potentiator.** (A) Representative I_{Na} in *WT*, *MCU*^{-/-}
727 and *EMRE*^{-/-} mitoplasts at 110 mM [Na⁺]_{cyto}. (B) I_{Na} amplitudes measured at -80 mV in *WT* ($n =$
728 20), *MCU*^{-/-} ($n = 3$) and *EMRE*^{-/-} ($n = 3$) mitoplasts. (C) Representative I_{Ca} (blue) and I_{Na} (red)
729 recorded from the same *WT* and *MICU1*^{-/-} mitoplasts exposed to 1 mM [Ca²⁺]_{cyto} or 110 mM
730 [Na⁺]_{cyto}. (D to F), Amplitudes of I_{Na} (D) and I_{Ca} (E), and the I_{Ca}/I_{Na} ratio in the same mitoplast
731 (F) in *WT* ($n = 27$) and *MICU1*^{-/-} ($n = 18$). Current were measured at -80 mV. Mean \pm SEM;
732 unpaired t-test, two-tailed. *** $p < 0.001$. (G) Inward I_{Na} recorded in the absence of cytosolic Ca²⁺
733 (blue) and subsequently at 2 nM [Ca²⁺]_{cyto} (red) in *WT* (left) and *MICU1*^{-/-} (right) mitoplasts
734 exposed to 110 mM [Na⁺]_{cyto}. (H) Inhibition of I_{Na} by 2 nM [Ca²⁺]_{cyto} in *WT* and *MICU1*^{-/-}. Mean \pm
735 SEM; unpaired t-test, two-tailed ($n = 4$ each).

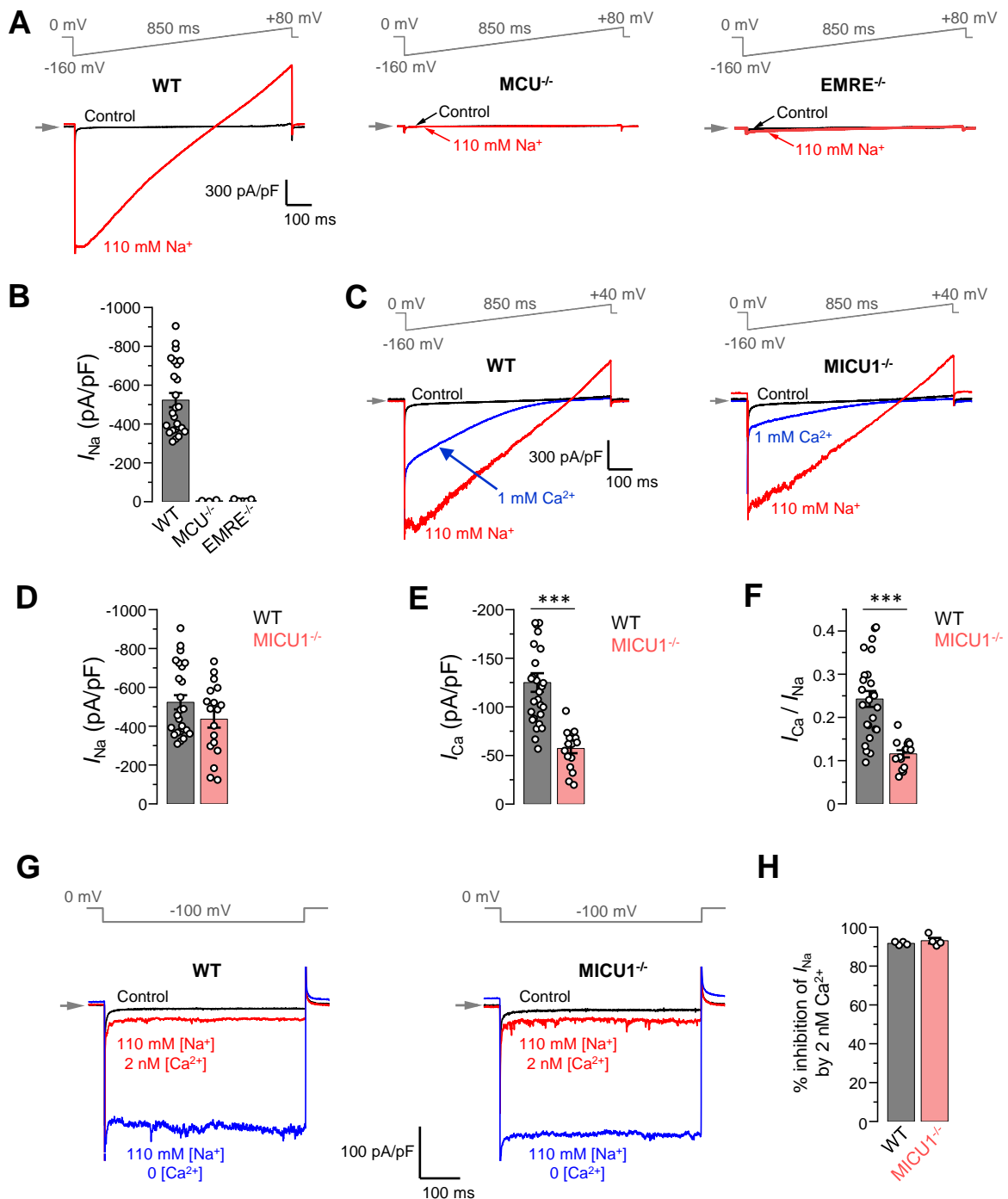


Fig. 2

736 **Fig. 3. Effects of MICU proteins and their EF hands on the amplitude, kinetics and**
737 **rectification of I_{Ca} .** (A) Western blots showing overexpression of MICU proteins or MICU
738 proteins with non-functional EF hands (mut-EF-MICU) in their respective knockout background
739 (left, $MICU1^{-/-}$; middle, $MICU2^{-/-}$ and; right, $MICU3^{-/-}$). (B to D) Upper panels: I_{Ca} in $MICU1^{-/-}$
740 (B), $MICU2^{-/-}$ (C) and $MICU3^{-/-}$ (D) before and after overexpression of a corresponding MICU
741 subunit or its EF hand mutant, as compared to *WT*. To simplify comparison, representative I_{Ca}
742 traces recorded from the mitoplasts of different backgrounds in 1 mM $[Ca^{2+}]_{cyto}$ are shown
743 together in a single panel. Lower panels: quantification of I_{Ca} amplitudes from the upper panel at
744 -160 mV. The same *WT* and knockout data were used as in Fig. 1e. Mean \pm SEM; one-way
745 ANOVA with post-hoc Tuckey test ($n = 7$ to 26). * $p < 0.05$; ** $p < 0.01$; *** $p < 0.001$. (E) Left
746 panel: I_{Ca} measured at a holding voltage of -100 mV while $[Ca^{2+}]_{cyto}$ was rapidly ($\tau \sim 0.4$ ms, see
747 Methods) switched from virtual zero to 1 mM and then back to virtual zero in *WT* (grey) and
748 $MICU1^{-/-}$ (red) mitoplasts. Right panel, I_{Ca} kinetics within ~ 10 ms after the fast $[Ca^{2+}]_{cyto}$
749 elevation and subsequent decrease in *WT* (grey) and $MICU1^{-/-}$ (red) mitoplasts from the left
750 panel. I_{Ca} traces were normalized to the maximal amplitude to facilitate comparison of kinetics in
751 *WT* and $MICU1^{-/-}$. (F) Left: I_{Ca} activation time constant (τ_a) in *WT* and $MICU1^{-/-}$; Right: I_{Ca}
752 deactivation time constant (τ_d) in *WT* and $MICU1^{-/-}$. Mean \pm SEM ($n = 3$, each). (G) I_{Ca} at
753 $[Ca^{2+}]_{mito} = 2$ mM and indicated $[Ca^{2+}]_{cyto}$ in *WT* and $MICU1^{-/-}$. Arrows point out where the
754 amplitude of outward I_{Ca} was measured. Bar-graph shows the amplitude of outward I_{Ca} measured
755 at +80 mV. $n = 3$, each $[Ca^{2+}]_{cyto}$.

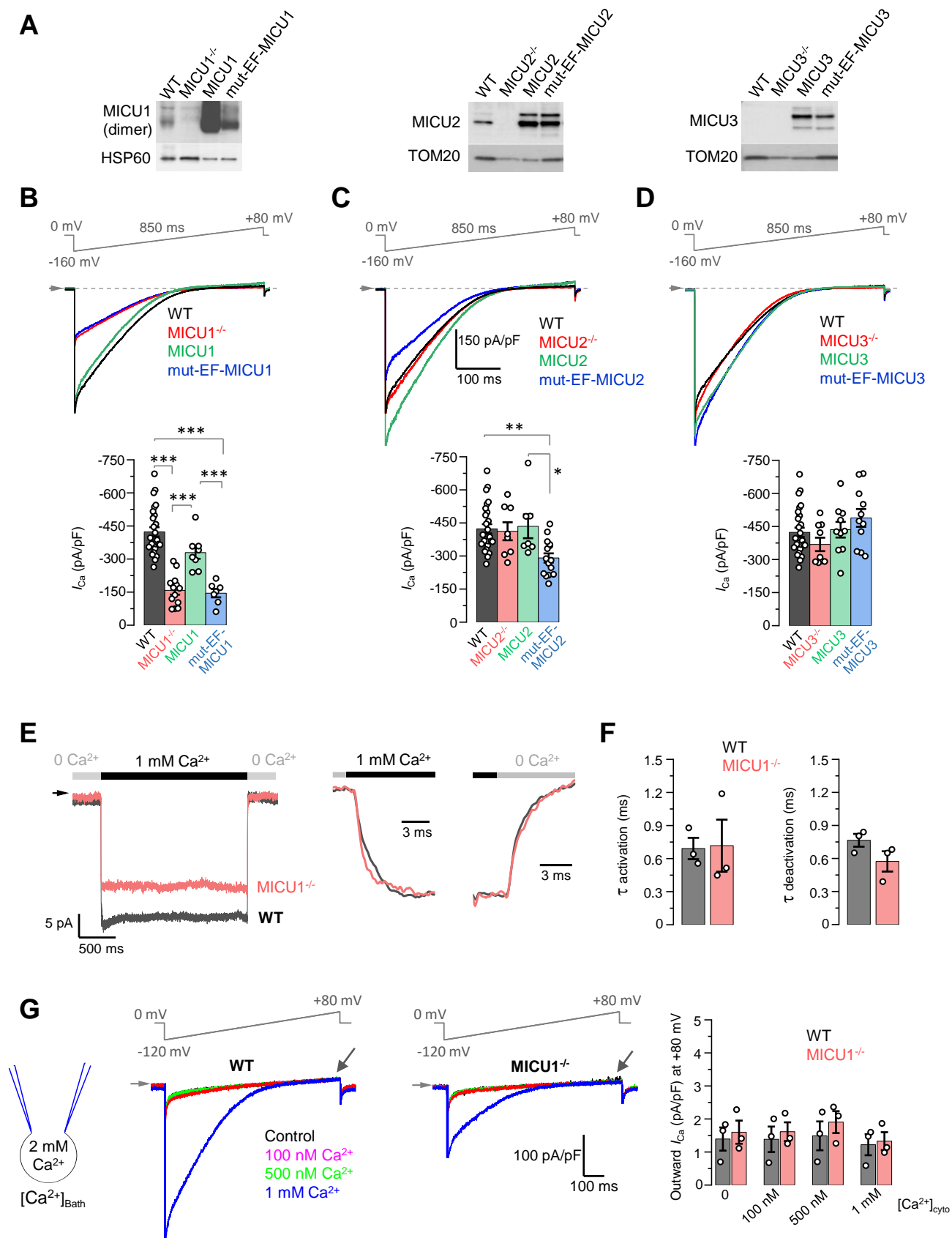


Fig. 3

756 **Fig. 4. Open probability of the MCU channel is decreased in *MICUI*^{-/-}.** (A and B) MCU
757 single-channel currents (i_{Ca}) from inside-out IMM patches in *WT* (A) and *MICUI*^{-/-} (B) recorded
758 at indicated potentials in symmetrical 105 mM Ca^{2+} , and low-pass filtered at 0.3 kHz for display
759 purposes. Arrows indicate closed state level, and downward deflections are the open state events.
760 Multiple subconductance levels are clearly visible at -80 and -120 mV. (C to E) Single-channel
761 amplitudes (C), open probability (P_o) (D), and time-averaged unitary current (E) (see Methods)
762 in *WT* and *MICUI*^{-/-} at indicated potentials. Mean \pm SEM; unpaired t-test, two-tailed; $n = 5-6$,
763 each. * $p < 0.05$; ** $p < 0.01$.

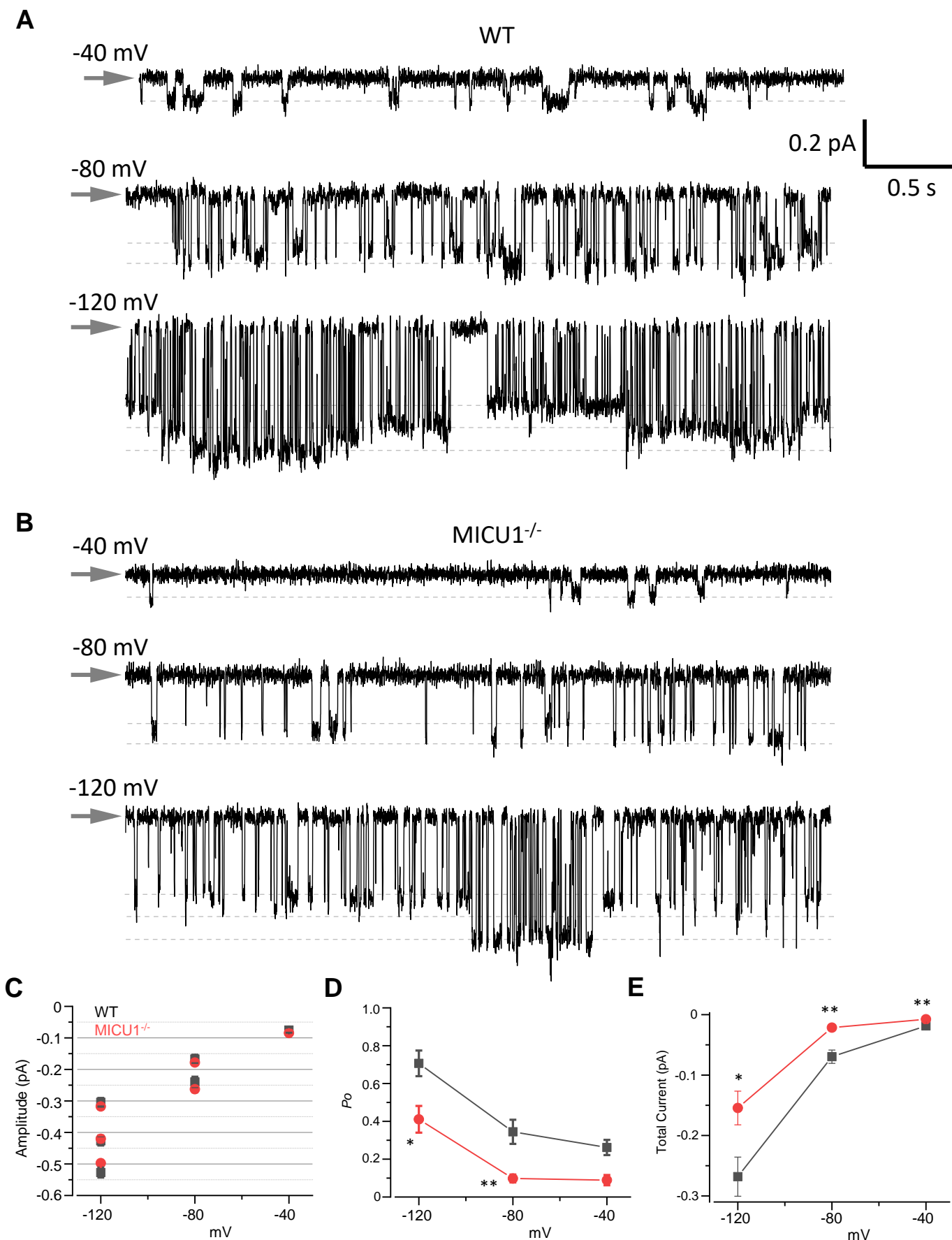


Fig. 4

764 **Fig. 5. I_{Mn} is reduced in $MICUI^{-/-}$ to the similar extent as I_{Ca} .** (A to C) Representative inward
765 I_{Mn} in *WT* (A), $MCU^{-/-}$ (B) and $EMRE^{-/-}$ (C) mitoplasts at 5 mM $[Mn^{2+}]_{cyto}$. (D) I_{Mn} measured at -
766 160 mV from *WT* ($n = 6$), $MCU^{-/-}$ ($n = 5$) and $EMRE^{-/-}$ ($n = 3$) mitoplasts. Mean \pm SEM. (E) I_{MCU}
767 amplitudes at 5 mM $[Ca^{2+}]_{cyto}$ and 5 mM $[Mn^{2+}]_{cyto}$ in *WT* mitoplasts. Currents were measured at
768 -160 mV. Mean \pm SEM; unpaired t-test, two-tailed; $n = 6-14$; *** $p < 0.001$. (F) Representative
769 I_{Ca} (blue, $[Ca^{2+}]_{cyto}=1$ mM), I_{Mn} (green, $[Mn^{2+}]_{cyto}=5$ mM) and inhibition of I_{Ca} by Mn^{2+} (red,
770 $[Ca^{2+}]_{cyto}=1$ mM and $[Mn^{2+}]_{cyto}=1$ mM) in *WT* and $MICUI^{-/-}$ mitoplasts. (G to J) I_{Mn} (G), I_{Ca} (H),
771 I_{Mn}/I_{Ca} ratio (I, measured in the same mitoplasts), and inhibition of I_{Ca} by 1 mM $[Mn^{2+}]_{cyto}$ (J) in
772 *WT* ($n = 3-6$) and $MICUI^{-/-}$ ($n = 5-11$). Mean \pm SEM; unpaired t-test, two-tailed. ** $p < 0.01$;
773 *** $p < 0.001$.

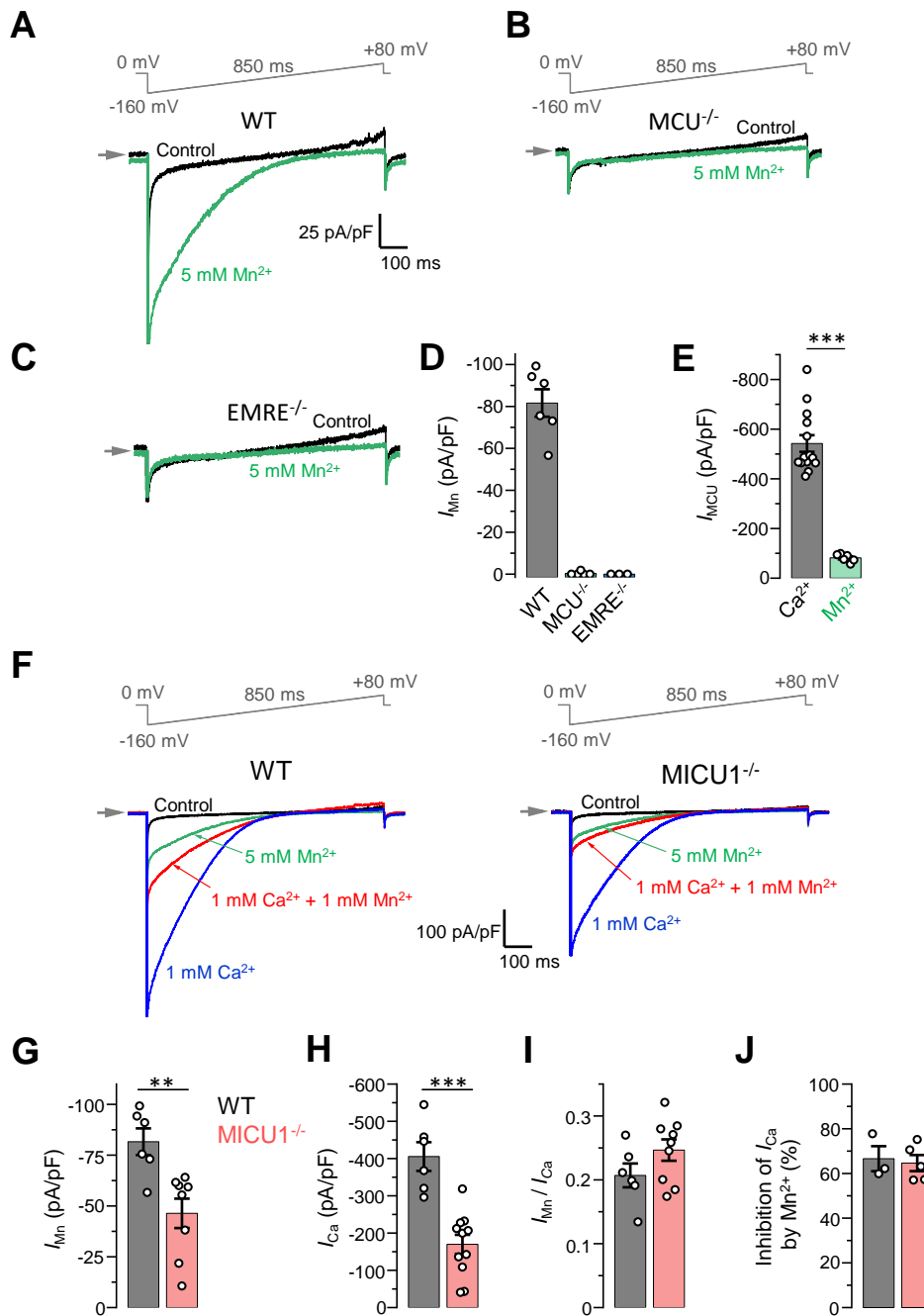
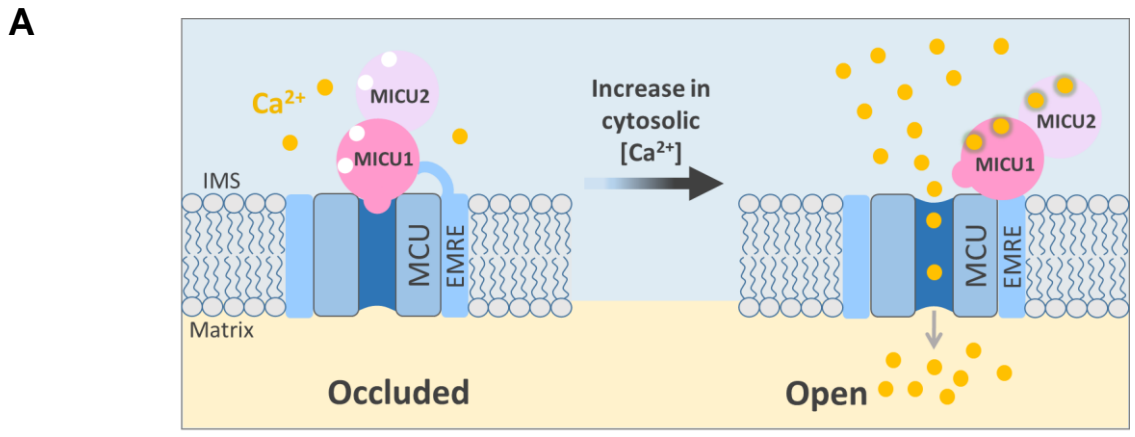
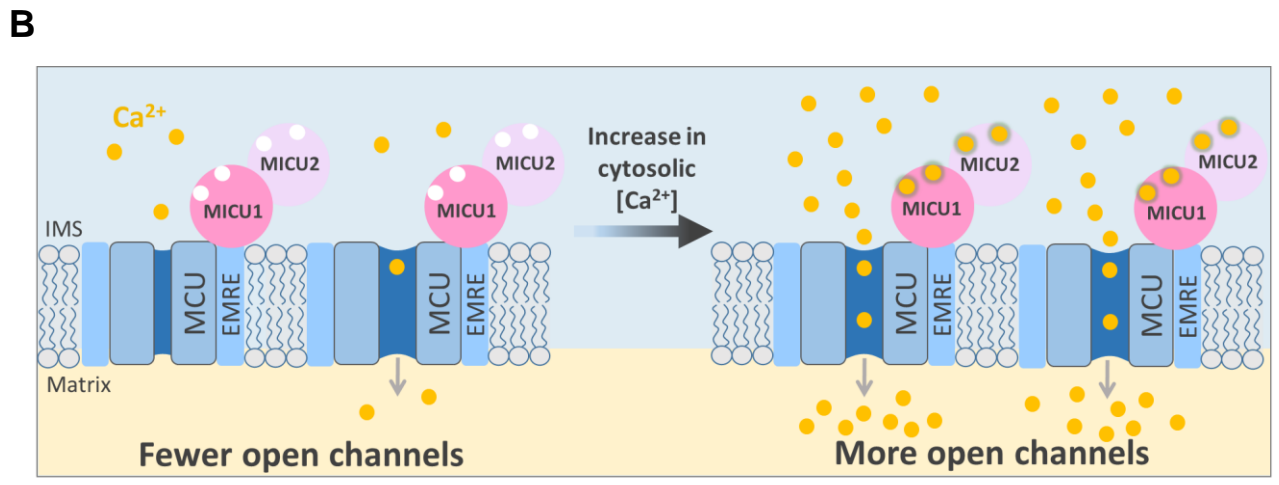


Fig. 5

774 **Fig. 6. Gating models of the MCU complex.** (A) Current model of the MCU complex gating
775 and the role of MICU subunits. The MCU complex has two states: MICU-occluded and open. At
776 low $[Ca^{2+}]_{cyto}$, MICU subunits occlude the MCU pore and inhibit Ca^{2+} influx. As $[Ca^{2+}]_{cyto}$ is
777 increased, Ca^{2+} binds to the EF hands of MICU subunits, the MICU-mediated occlusion is
778 relieved, and the MCU pore is open. (B) New model of the MCU complex gating and the role of
779 MICU subunits. The MCU complex is a constitutively active channel. The level of the MCU
780 activity is determined by spontaneous transitions between the open and closed states and the
781 equilibrium between them. At low $[Ca^{2+}]_{cyto}$, this equilibrium is such that the probability of the
782 open and closed states are comparable. As $[Ca^{2+}]_{cyto}$ is increased and Ca^{2+} binds to the EF hands
783 of MICU subunits, MICUs strongly shift the equilibrium to the open state, which leads to a
784 significant increase in the probability of the open state (P_o) and a robust increase in the MCU
785 activity.



Old MCU Gating Model



New MCU Gating Model

Fig. 6